nature communications

Article

https://doi.org/10.1038/s41467-025-68088-3

Highly reconfigurable neuronlike conductive networks through nanophase structure engineering

Received: 30 May 2025

Accepted: 17 December 2025

Published online: 29 December 2025

Check for updates

Wei Zhong[1,4], Haojie Zhao[1,4], Bowen Yao[1,4] ✉, Zhenze Li[2], Shuai Zhou[1], Zhifeng Wang[3], Yuhao Geng[1], Wen Sun[1] & Jiajun Fu[1] ✉

Bionic electronics are designed to bridge the gap between biological systems and conventional electronic devices. However, replicating the high dynamic adaptivity and functional plasticity of living tissues while preserving the electrical performance and structural integrity of traditional electronics remains highly challenging, owing to the intrinsic trade-offs in molecular design. To address this issue, a methodology of reversible nanophase regulation is proposed, inspired by ion-specific effects in biological environments. Benefiting from the dynamic response of noncovalent interaction to specific ions, the developed system can successfully integrate multiple traditionally contradictory properties–combining outstanding electrical/mechanical performance with excellent reconfigurability, such as re-writability of conductive pathways, in-situ wet solderability with good spatial resolution, and closed-loop recyclability. This methodology offers a promising framework for designing reconfigurable devices for bioelectronics applications such as human-machine integration and tissue engineering.

Bionic electronics aim to merge biological living organisms and conventional electronic devices, with great promise in applications such as wearable/implantable intelligent devices[1], tissue engineering[2], human-machine interaction[3], and neurorobotics[4]. However, most conventional electronic devices struggle to replicate the intrinsic reconfigurability and responsiveness of biological living tissues at the hardware level[5–7]. For example, the brains encode and remove memories by strengthening or weakening synaptic connections between neurons through trans-synaptic proteins such as neurexins (presynaptic) and neuroligins (postsynaptic)[8,9] (Fig. 1a). In contrast, traditional electronics are typically incapable of reconfiguring their circuitry once fabricated, resulting in limited functional plasticity across spatial and temporal dimensions.

To offer reconfigurability to electronics, two strategies at different spatial scales were proposed, *i.e.*, macroscopic geometric regulation and molecular structure (or doping level) regulation. Based on these two strategies, several reconfigurable devices were developed, with examples ranging from the adjustable antennae based on mechanical stretching[10,11], rewritable conductive hydrogel by controlling their swelling degrees[12–15] to active optical metasurface devices based on dynamic conducting polymer[16,17] and neuromorphic devices by engineering ion migration and electron transport[18–20]. Unfortunately, these two strategies struggled to integrate reconfigurability with excellent electrical performance and size scalability, inferior to bulky but delicate living organisms. This issue is mainly rooted in an intrinsic conflict in material design, where the high electrical performance usually requires electrical materials to have highly conjugated or crystalline molecular structures with intimate electrical contacts, while the high reconfigurability usually necessitates weak and responsive intermolecular interaction. For instance, light-responsive conductive hydrogel could be constructed through host-guest interaction, but suffered from a low electrical conductance or structural

[1]School of Chemical Engineering, Nanjing University of Science and Technology, Nanjing, China. [2]Department of Precision Instrument, Tsinghua University, Beijing, China. [3]Testing Center, Yangzhou University, Yangzhou, China. [4]These authors contributed equally: Wei Zhong, Haojie Zhao, Bowen Yao.
✉e-mail: bowenyao@njust.edu.cn; fujiajun668@njust.edu.cn

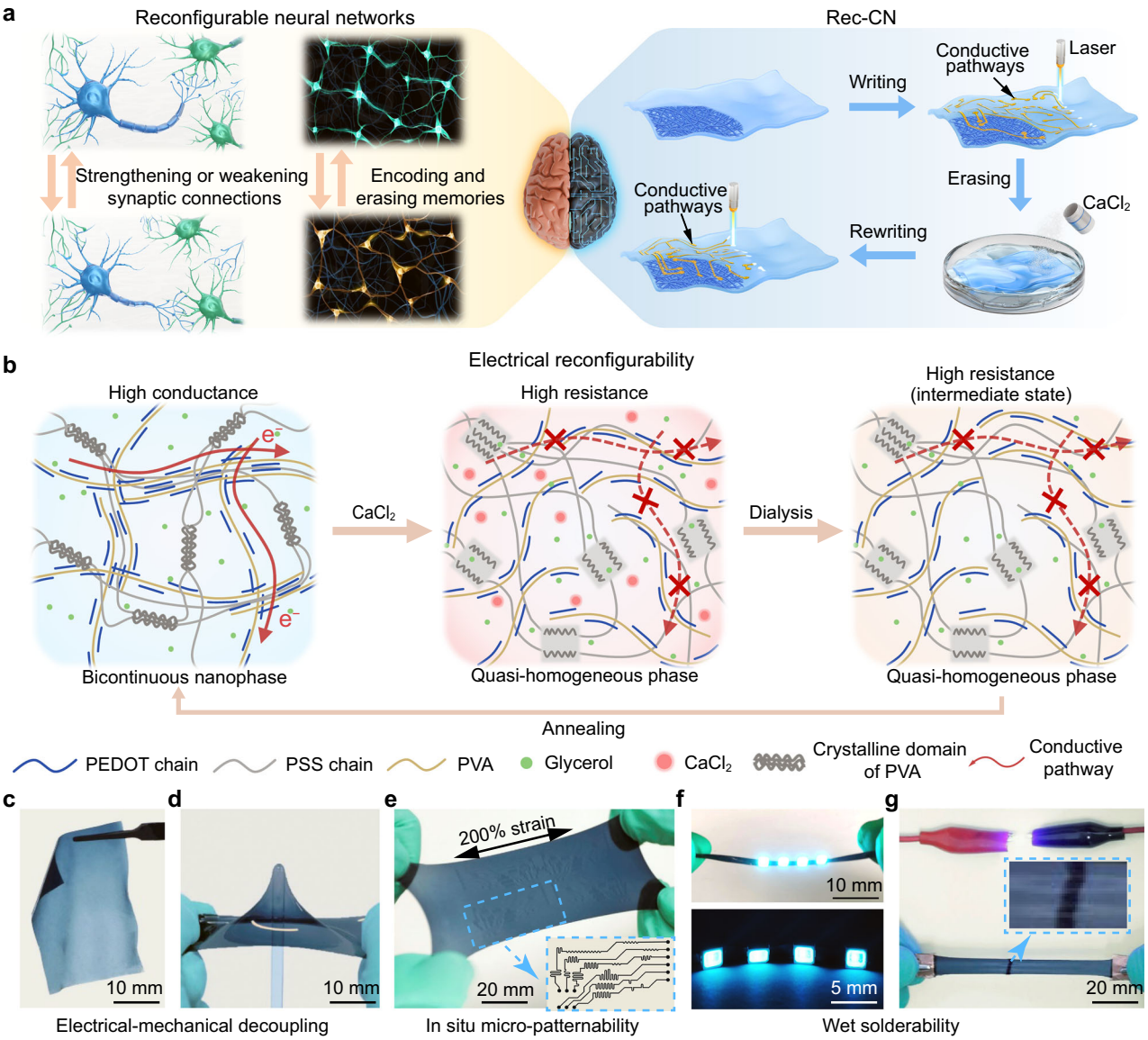

Fig. 1 | Design and unique features of Rec-CN. a Schematics of neural circuitry and Rec-CN. The brain encodes and removes memory by altering the neural interconnections. Analogously, the Rec-CN can be repeatedly micro-patterned through laser irradiation and salt treatment without compromising its structural integrity. **b** Schematics showing the evolution of nanophase structure and conductive pathway within a CP-PVA organogel upon different treatments. **c**–**g** Digital photographs of the CP-PVA organogel, demonstrating its high mechanical toughness, re-writability of conductive pathways, and in-situ wet solderability. The inset in panel **e** represents the circuit diagram of the conductive pathways. In **f**, **g** CP-PVA organogel strips were soldered to metal pins (**f**) or to themselves (**g**), and used to power connect light-emitting diodes (LEDs) upon a constant current of 20 mA.

compactness[15]. Therefore, bionic reconfigurable electronics sharing a similar physiological mechanism to organisms are highly demanded and challenging.

The specific ion effect, encompassing the popular Hofmeister series, has long been found to strongly affect a range of biological processes such as neuron activity, mainly originating from electrostatic interaction, hydration effects, and/or molecular sieve effects[21,22]. Inspired by this biological mechanism, we herein propose a general strategy, reversible nanophase regulation of non-covalent crosslinking networks, to successfully construct neuron-mimicking highly-reconfigurable conductive networks (Rec-CN) (Fig. 1a). As an exemplary model, physically crosslinked conductive networks are prepared with conducting polymer, poly(3,4-ethylenedioxythiophene): polystyrene sulfonate (PEDOT:PSS, CP), and polyvinyl alcohol (PVA) as building blocks (Fig. 1b). By leveraging specific ion effect, the conductive network could be finely engineered, either locally or globally, to transition among different thermodynamic states with different nanophase structures, driven by the delicate balance of inter- and intra-molecular non-covalent interactions of polymers (Fig. 1b). The unique capability enabled controlled spatial modulation of electrical conductivity within a single system over a remarkable range of 4–5 orders of magnitude, without compromising structural integrity and mechanical robustness (Fig. 1c–e).

Moreover, owing to the high reconfigurability, in-situ wet soldering and closed-loop recycling could also be realized. In the in-situ wet soldering, the Rec-CN could be directly joined to diverse substrates via laser process or thermal treatment, while preserving its multichannel electrical connections and 3-dimensional (3D) geometric integrity, standing in contrast to previously reported hydrogel soldering methods, which typically required intricate manual operation or were incompatible with 3D gels (Fig. 1f, g)[23]. In the closed-loop recycling, the Rec-CN could also be recycled in a nearly closed loop

through dialysis and heating, with no significant loss in mechanical and electrical properties. Last, benefiting from these unique features, the Rec-CN were therefore demonstrated for the application of various bioelectronics and wearable electronics, including a reconfigurable printing circuit board (Rec-PCB), an on-body wrist for electrophysiological signal capture, and rewritable electroluminescent devices.

As a whole, we propose a reversible nanophase regulation strategy to address a critical methodology gap in bridging the spatial scales for the in-situ regulation of electrical performance in reconfigurable electronics. As a result, this approach successfully integrates good electrical and mechanical performance with outstanding reconfigurability features, such as micro-pattern ability and re-writability of conductive pathways, in-situ wet solderability with good spatial resolution, and closed-loop recyclability. This strategy also shows great compatibility with other material systems, such as metal-based elastomers and insulative components with ion-specific effects, shedding light on the design of bionic next-generation electronics. Additionally, this work successfully demonstrates that specific ion effects can be utilized to delicately in situ tune the physical properties of noncovalent networks through nanophase structure engineering, providing an efficient toolbox for the mechanism study of polymer-based functional composites, especially for the volatile or degradable system where the employment of the conventional time-temperature superposition principle may be restrained.

Results

Material design, electrical, and mechanical performances

Conductive organogels were constructed as exemplary reconfigurable models by employing CP, PVA, and glycerol as conductive filler, phase-regulating components, and dispersed medium, respectively. In mechanism design, CP and PVA were able to offer abundant hydrogen bonds and electrostatic interactions that were susceptible to specific ion effects, thus benefiting the reconfigurability of polymer networks, whereas glycerol could serve as both a plasticizer to prevent over-dense stacking of CP and PVA for higher dynamics and a lowly volatile medium for expanded working temperature windows. Unless otherwise specified, for the preparation of the organogels, suspensions containing different ratios of CP and PVA, with 4 wt% glycerol, were drop-casted on substrates and then partially dried under ambient conditions (25 °C, 50% relative humidity) for 24 h. During this drying process, most water was selectively evaporated, leaving behind pristine CP-PVA organogels (p-CP-PVA) with solid contents of ~40 wt% and residual water contents of 22 wt% (relative to the total mass of organogels) (Supplementary Fig. 1). The influence of environmental humidity during drying is discussed in Supplementary Note 1 and summarized in Supplementary Table 1.

The p-CP-PVA organogels were free-standing and exhibited varied mechanical robustness depending on the relative contents of each component (Supplementary Note 2 and Supplementary Figs. 2–4). For the electrical performance, the p-CP-PVA organogels were almost non-electronically-conductive, as measured by a significantly low conductivity of 0.46–0.73 mS cm^{-1} (Supplementary Fig. 5). To improve the conductance, mild thermal annealing was implemented in ambient environment, with an optimum annealing temperature of 80 °C and duration of 2 h selected based on organogel stability and experimental reproducibility (Supplementary Note 3, Supplementary Fig. 6). The resultant organogels (CP-PVA) experienced significant improvement by 4–5 orders of magnitude, reaching 4.6-112.5 S cm^{-1} depending on the CP's contents in the organogels, accompanied by moderate improvement in mechanical performance and increase in solid content of ~50 wt% (Fig. 2a–d and Supplementary Figs. 6 and 7). Notably, the thermal annealing was largely insensitive to environmental humidity, as revealed by the comparable low residual water contents (~4%) in organogels treated under different relative humidity levels (20–70%) (Supplementary Note 1, Supplementary Fig. 8 and Supplementary Table. 1). Moreover, the conductivities of organogels showed low dependency on the gel thickness in a wide range of 0.3–1.0 μm, confirming the uniform distribution of CP within the organogel matrix (Supplementary Note 4 and Supplementary Fig. 9).

More importantly, when compared with the pure PVA organogel, the thermally-annealed CP-PVA organogel exhibited unexpected improvement in mechanical performance, which is in sharp contrast to most previous reports where the incorporation of rigid conductive fillers typically led to embrittlement of the composites (See detailed comparison in Supplementary Table 2). Specifically, with increasing the CP content from 0 to 16 wt% (relative to the total mass of CP and PVA), the CP-PVA organogels exhibited simultaneous increases in Young's modulus, fracture strain, strength, and toughness by 208.3% (2.4–7.4 MPa), 30.4% (761–992%), 70.6% (6.8–11.6 MPa) and 145.5% (32.5–79.8 MJ m^{-3}), respectively (Fig. 2c, d, Supplementary Fig. 7). As a result, the PVA-CP organogels exhibited superior comprehensive performance in terms of conductivity, stretchability, and toughness when compared with previously reported conducting polymer hydrogels (Fig. 2e, f, Supplementary Fig. 10 and Supplementary Table 3). Furthermore, the CP-PVA organogels exhibited satisfactory conductance retention upon tensile strain, as shown by low increases in resistance by only 0.04, 0.22, and 1.20 times at the strains of 50%, 100%, and 200%, respectively (Supplementary Fig. 11).

At last, the CP-PVA organogels exhibited higher resistance to environmental humidity and high/low temperature than their hydrogel counterpart with only water as the dispersed medium, due to the low volatility of glycerol (Supplementary Figs. 12–20 and Supplementary Note 5). For example, upon exposure to a high-temperature environment of 80 °C, the CP-PVA organogels showed satisfactory stability in terms of mechanical and electrical properties. Such high intactness could not only enhance the system's reliability but also greatly expand the methodological toolbox for rational control over the conductive network by regulating nanophase structure, a key for the reconfigurable system as elaborated below.

Mechanism for the formation of bicontinuous phase

The successful decoupling of electrical and mechanical performances of the CP-PVA organogel could be attributed to the formation of a bicontinuous nanophase structure composed of PVA-rich and CP-rich domains. This unique nanophase structure was a thermodynamically favored state as a delicate balance between the miscibility and self-aggregability of the CP and PVA chains in the glycerol medium, driven by hydrogen bonds and π-π interaction. On the one hand, both PVA and CP chains were prone to self-assemble themselves solely especially after thermal annealing at 80 °C (Fig. 2g and Supplementary Fig. 21). The thermal annealing could significantly activate the segmental motion of PVA and CP by partially dissociating the hydrogen bonds (Fig. 2h and Supplementary Fig. 22), leading to more ordered molecular configurations as revealed by X-ray diffraction (XRD) spectra of PVA and Raman spectra of CP (Fig. 2i and Supplementary Fig. 23). On the others, the PVA and PSS chains in CP could strongly interact with each other through ionic hydrogen bonds, according to dynamic light scattering (DLS) spectra, Fourier-transform infrared (FT-IR), XRD spectra and mechanical tests (Fig. 2j, Supplementary Figs. 24–28, Supplementary Table 4). Furthermore, the glycerol, serving as an effective plasticizer through multiple hydrogen-bond interactions with both PVA and CP, could greatly suppress dense self-aggregation and thus enhance the polymer miscibility (Supplementary Fig. 29)[24].

With the synergy of the two opposite tendencies as mentioned above, phase separation on the nanometer scale, therefore, occurred within the PVA-CP organogels, leading to the formation of a bicontinuous phase structure composed of PVA- and CP-rich domains. In detail, after thermal annealing, the CP-PVA organogels exhibited an

https://doi.org/10.1038/s41467-025-68088-3

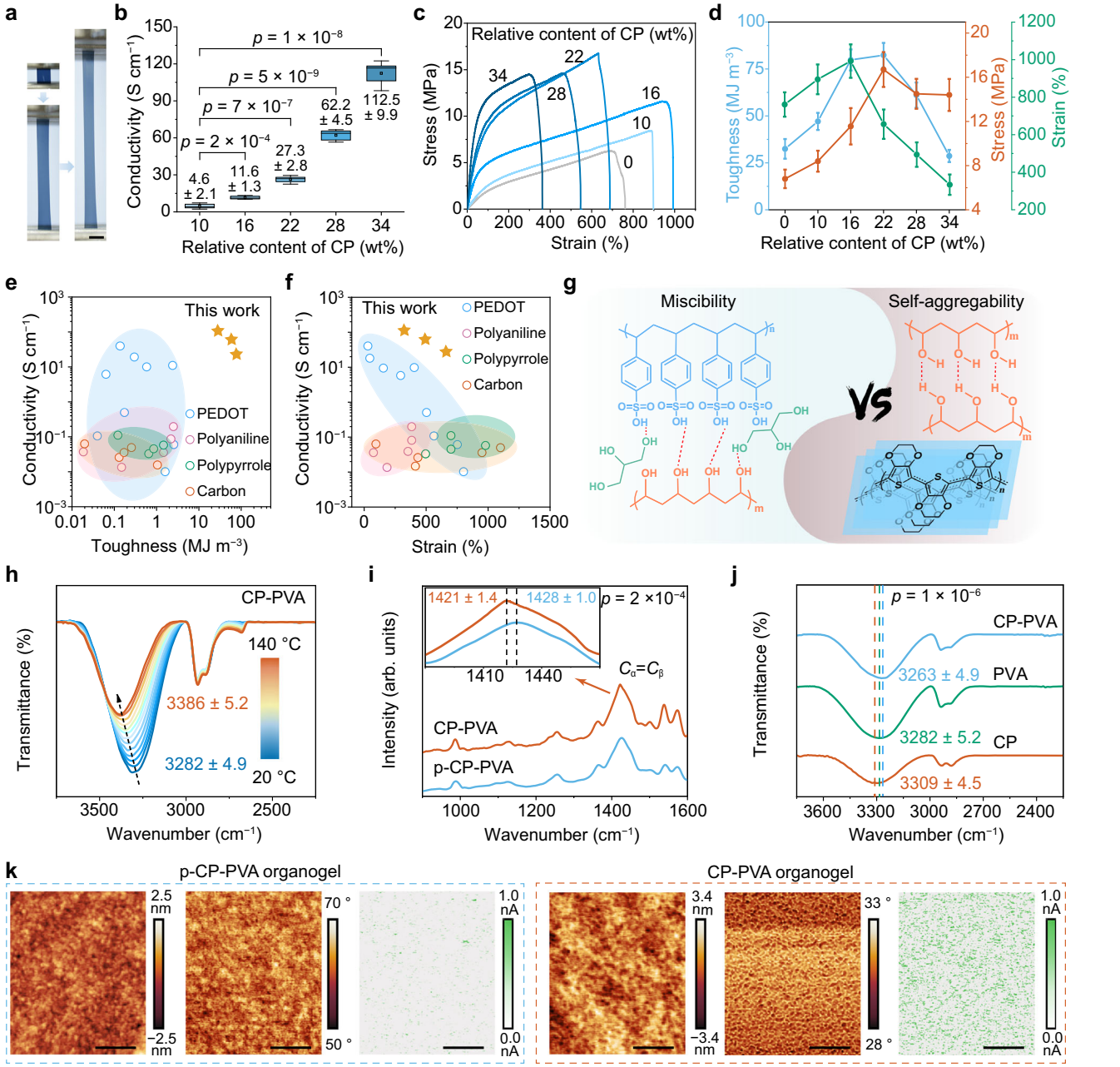

Fig. 2 | Decoupling of mechanical and electrical performance. a Digital photograph of CP-PVA organogel stretched to 10 times the original length (scale bar = 15 mm). Conductivity (**b**), tensile stress-strain curves (**c**), and performance comparison (**d**) of CP-PVA organogels with different contents of CP (relative to the total mass of PVA and CP) (strain rate: 200% min^{-1}). Data in panel **b** are presented in box-and-whisker plots, where the central dots, lines, and box limits indicate the mean, the median, and the upper/lower quartiles, and the whiskers extend to 1.5× the interquartile range from the quartiles (sample size = 4). **e**, **f** Ashby plots comparing the toughness, strain, and conductivity of CP-PVA organogels with previously reported hydrogels. Data points are obtained from references mentioned in Supplementary Fig. 10 and Supplementary Table 3. **g** Schematic illustration showing the balance between miscibility and self-aggregability of polymers. Temperature-dependent FT-IR spectra (**h**), Raman spectra (**i**), and ordinary FT-IR spectra (**j**) of different organogels. **k** AFM characterizations of p-CP-PVA and CP-PVA organogels: height image (left panel), phase image (middle panel), and tunneling current image recorded in TUNA (tunneling AFM) mode (right panel) (scale bar = 500 nm). Data in panels **d**, **h**-**j** were presented as mean values ± standard deviation (mean ± s.d.) (sample size = 4). Statistical significance was assessed using two-sided *t-tests* for comparisons between two groups (**b**, **i**), and one-way analysis of variance (ANOVA) for comparisons among multiple groups (panel **j**), with significance determined by *p* values. Unless otherwise specified, CP-PVA organogels with a solid content of ~50 wt% (relative to the total mass of organogels) and CP's content of 22 wt% (relative to the total mass of CP and PVA) were used here.

improved degree of nanophase separation as shown by a significantly decreased interphase distance with high contrast in the phase images according to atomic force microscopy (AFM) characterizations (Fig. 2k). The nanophase separation structure could greatly benefit the electrical interconnection of CP chains while preventing their over-aggregation, thus leading to a uniform conductive percolation network throughout the PVA matrix. Additionally, the phase separation degree was quantified by small-angle X-ray scattering (SAXS). In SAXS, the scattering peak of PVA-CP organogels turned more pronounced with a positive shift after thermal annealing, corresponding to a decrease in the average interphase distance from 10.6 to 8.2 nm (Supplementary Fig. 30).

Worthy to note, the bicontinuous nanophase was thermodynamically favored in the glycerol medium and could be regulated by altering the chain mobility and intermolecular interaction (this will be discussed in the following). As a whole, driven by the hydrogen bonds, π-π stacking, and hydrophobic interaction, a delicate balance between the miscibility and self-aggregability of the CP and PVA chains was realized, thus leading to a bicontinuous nanophase structure composed of PVA- and CP-rich domains, where the former accounts for mechanical performance and the latter is responsible for electrical performance. The phase separation on the nanoscale could ensure the uniform distribution of conductive percolation networks and stress transfer pathways, thus rendering a successful integration of excellent electrical and mechanical performances (toughness).

Regulable conductance through the specific ion effect

Given that it is bicontinuous nanophases accounting for the successful decoupling of electrical and mechanical performance, the CP-PVA organogels' conductance was therefore expected to be regulable if the nanophase structure could be engineered on demand. Herein, this hypothesis was successfully verified by introducing the specific ion effect into the organogel system. Specific ion effects, encompassing the Hofmeister series, originally describe a persistent trend in the effect of ions on the secondary structure and dispersibility of bio-macromolecules[21]. In general, cations with high charge density or anions with low charge density usually lead to higher solvation degrees of bio-macromolecules, while cations with low charge density or anions with high charge density often induce opposite effects. A widely accepted mechanism behind this phenomenon involves the ions impacting the solvation shell of molecules by electrostatic and polarization effects[25]. This phenomenon has also been extended to hydrogel systems recently, with examples including PVA[26], polyampholyte[27], and poly(N-isopropylacrylamide) (PNIPAm) hydrogels[28]. These hydrogels exhibited regulable mechanical properties (*e.g.*, Young's modulus) depending on the types of ions introduced in the system[29].

For the CP-PVA organogels developed here, their conductance showed a high dependency on the types of ions introduced. Overall, cations showed a pronounced impact on the conductance of the organogels, following a similar ranking to the traditional Hofmeister series, whilst anions imposed a weak influence (Fig. 3a, b). Particularly, after being subject to treatment with glycerol solution containing 2 mol L^{-1} $CaCl_2$ for 3 days (followed by selective evaporation at an ambient environment to evaporate most of the water), the CP-PVA conductive organogels transformed from a high-conductance state (27.3 S cm^{-1}) (denoted as State I) to a high-resistance state (1.9×10^{-2} S cm^{-1}) (denoted as State II) (Fig. 3c and Supplementary Fig. 31). This transition also reduced the Young's modulus and toughness by 62 and 30%, respectively, with a slight change in solid content (51–44 wt%; Supplementary Fig. 32). Furthermore, the resistance of State II was maintained or even further increased by dialyzing out Ca^{2+} ion with glycerol solution, followed by selective evaporation at an ambient environment, to produce State III (residual Ca^{2+} ion content: ~0.5% relative to the carbon, Supplementary Figs. 31, 33 and Supplementary Table 5). In this state, the conductivity decreased to 3.3×10^{-3} S cm^{-1}, while the mechanical performance and solid content remained stable. Moreover, State III could be reverted to the original high-conductance state by thermal annealing at 80 °C for 2 h (State I_2), recovering the initial electrical and mechanical performance (Supplementary Figs. 31, 32). Therefore, this process established a closed regulatory cycle with a high conductance on/off ratio (defined as the conductivity ratio of State I to State III). Furthermore, this cycle could be repeated several times with no significant alteration in the electrical performance (Supplementary Fig. 34).

Mechanism and generality of nanophase reconfiguration

Such excellent adjustability of conductance could be ascribed to the reversible swinging of the nanophase structure within the CP-PVA organogels in three different thermodynamic states, highly distinct from previously reported cases in which conductance reconfiguration of gels commonly relied on swelling/deswelling of the system[30] (Fig. 3d). In detail, firstly, the organogel in State I exhibited a bi-continuous phase structure as discussed in the above section, and should be thermodynamically favored given that thermal annealing was applied. Secondly, for State II, the bi-continuous phase was erased through Ca^{2+} treatment driven by thermodynamics. In detail, despite the Ca^{2+} could induce ionic crosslinking among partial PSS chains (Supplementary Fig. 35), these kosmotropic cations simultaneously interact with PVA chains, breaking the hydrogen bonds among them, as confirmed by FT-IR, XRD, and SAXS spectra (Fig. 3e and Supplementary Figs. 36, 37)[29]. The decrosslinking effect predominated over the ionic crosslinking, thereby enhancing the immiscibility of PVA and CP chains. As a result, the bi-continuous phase structure within the organogels was transformed into a more homogenous phase structure, leading to a highly resistive State II in the CP-PVA organogels. It is worth noting that such transformation should not be ascribed to the swelling of organogels, as no significant change in organogels' solid contents was observed (selective evaporation at an ambient environment were implemented to evaporate most of the water absorbed during salt treatment before resistance measurement) (Supplementary Fig. 31). Moreover, the State II was also thermodynamically favored, as proved by the negligible change in resistance of the organogel containing $CaCl_2$ after being subjected to thermal annealing at a high temperature of 60 °C for 5 h (Supplementary Fig. 38). In addition, according to X-ray photoelectron spectroscopy, approximately 25% of PSS was removed during $CaCl_2$ treatment in the first cycle, further supporting that nanophase structural was the primary factors governing the electrical properties, rather than compositional variations (Supplementary Fig. 39).

Thirdly, unlike the thermodynamically stable States I and II, State III was thermodynamically unstable but kinetically stable. The CP-PVA organogels after dialysis could remain highly resistant for a long duration at room temperature (*e.g.*, 25 °C for more than 7 days) (Fig. 3f). Such good kinetic stability could be attributed to the low chain mobility seriously retarded by hydrogen bonds among PVA and PSS chains. Subsequently, because of its thermodynamic instability, the organogel without $CaCl_2$ could be transformed back to a high conductance state (State I_2) through thermal annealing at a high temperature of 80 °C for 2 h, accompanied by the recovery of bi-continuous structure, as proved by AFM images, SAXS, and XRD spectra (Fig. 3e, g, and Supplementary Fig. 37).

Therefore, by harnessing the specific ion effect on the dynamic non-covalent interactions among polymer chains, reversible control over the organogels' conductance with a high on-off ratio was successfully achieved. To further validate this mechanism, three sets of control samples were prepared, including CP-PVA organogels with varying CP contents or solid contents, CP-PVA hydrogels or organogels derived from other organic solvents, and chemically crosslinkable CP-PVA_{MA} organogels (PVA_{MA}: methacrylate modified PVA) (Supplementary Figs. 40–53). The detailed discussion is provided in Supplementary Note 6. In brief, the control experiments further proved that the electrical reconfigurability originated from the dynamic response of polymers. Specially, organogels remained high on/off ratios of 10^3-10^4 across a wide range of CP content, but the ratio declined markedly at high loadings beyond a critical threshold of 34 wt% (Fig. 3h). Moreover, the conductance on/off ratio strongly correlated with the plasticization ability of dispersion media (solvent) in the organogels, specifically the hydrogen-bond-related Hansen solubility parameter (δ_h). Solvents with higher δ_h, which could offer more hydroxy groups for interaction with PSS and PVA[24], impart greater adaptability to the polymer network, thereby enhancing the electrical reconfigurability of corresponding organogels (Fig. 3i, Supplementary Figs. 51–53 and Supplementary Table 6). Notably, in contrast to the previously

https://doi.org/10.1038/s41467-025-68088-3

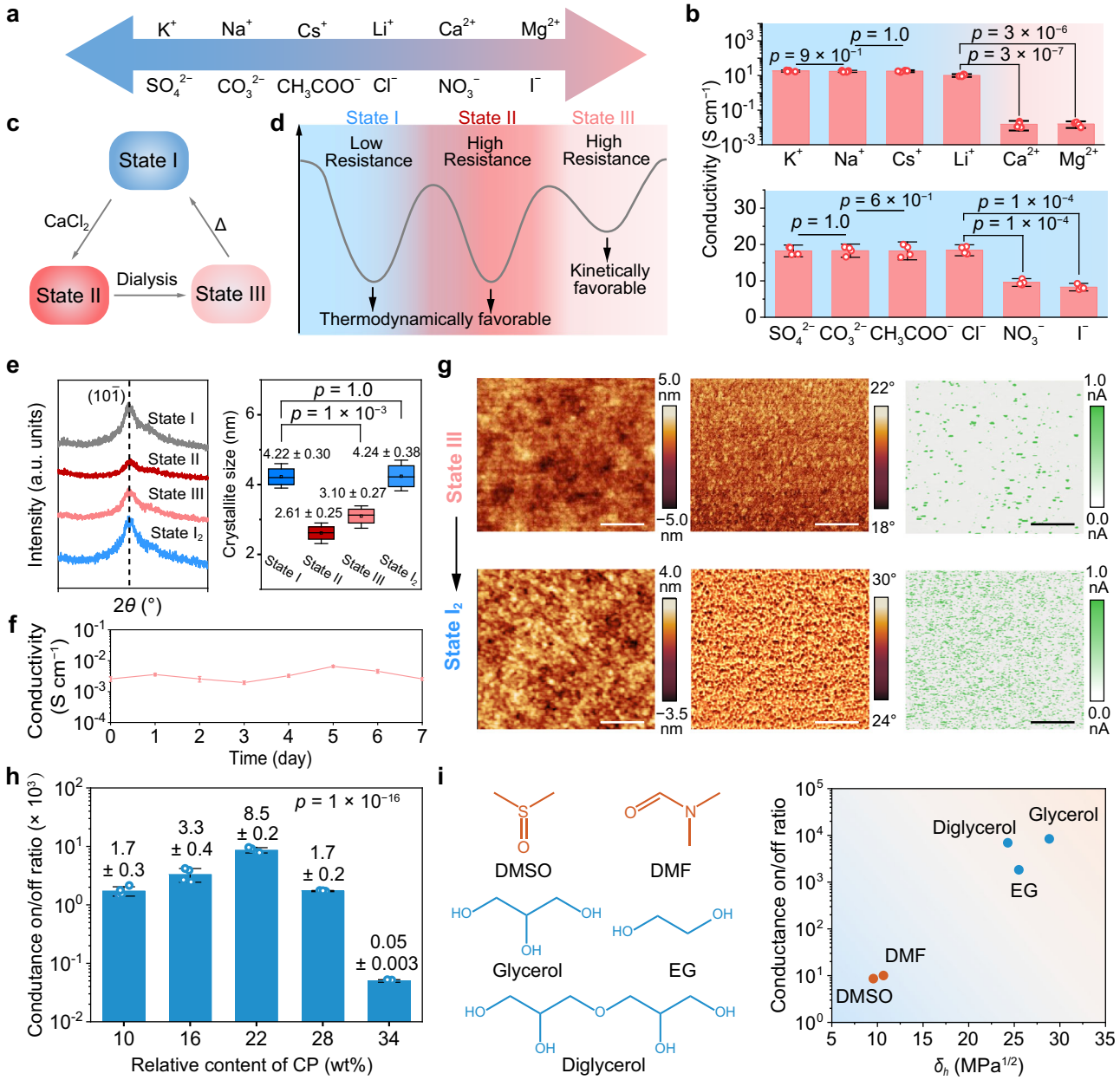

Fig. 3 | Nanophase reconfiguration of organogels. a Specific-ion series ranked according to the conductance change ratio of CP-PVA organogels after ionic treatment. **b** Conductivity of CP-PVA organogels after salt treatments (Cl^- and Na^+ served as counter ions, respectively). **c**, **d** Reversible regulation of CP-PVA organogels among three distinct thermodynamic states. **e** XRD patterns (left panel) of CP-PVA organogels at different states and average crystalline size (right panel) calculated from the (10$\bar{1}$) peak at 19.5°. The data in the right panel were presented in box-and-whisker plots, where the central dots, lines, and box limits indicate the mean, the median, and the upper/lower quartiles, and the whiskers extend to 1.5× the interquartile range from the quartiles (sample size = 4). **f** Conductance stability of CP-PVA organogel at State III, stored at ambient environments for different durations. **g** AFM characterizations of CP-PVA organogels at different states: height image (left panel), phase image (middle panel), and tunneling current image (right panel) (scale bar = 500 nm). **h** Conductance on/off ratio (conductance ratio of State I to State III) of CP-PVA organogels with varied contents of CP in the first switching cycle. **i** Conductance on/off ratio of CP-PVA organogels derived from various solvents serving as dispersion media. The data in **b**, **e**, **f**, **h** are presented as mean ± s.d. ($n = 4$). Statistical significance was assessed using two-sided *t*-tests for comparisons between two groups (**b**, **e** (right panel)), and one-way ANOVA for comparisons among multiple groups (panel **h**), with significance determined by *p* values. Unless otherwise specified, CP-PVA organogels with a solid content of ~50 wt% (relative to the total mass of organogels) and CP's content of 22 wt% (relative to the total mass of CP and PVA) were used for the tests here.

reported cases in pure PVA hydrogel system[29], cations showed a significantly stronger influence on the CP-PVA organogels than that of anions, as discussed above. This abnormal phenomenon suggested that the negatively charged CP (PEDOT:PSS) probably inhibited the anion penetration through electrostatic repulsion.

At last, the proposed electrical reconfiguration strategy showed good generality across different grades of PEDOT:PSS, alternative conductive fillers, and mechanical matrices (Supplementary Note 7, Supplementary Figs. 54–56). For example, the conductance reconfiguration was successfully achieved in organogels incorporating PEDOT:PSS with varying PSS contents (PEDOT:PSS ratios ≤ 1:3) or employing other ion-sensitive mechanical components (*e.g.*, polyacrylamide and PNIPAm). In addition, the conductance on/off ratios of CP-PVA organogels remained stable across a wide range of

https://doi.org/10.1038/s41467-025-68088-3

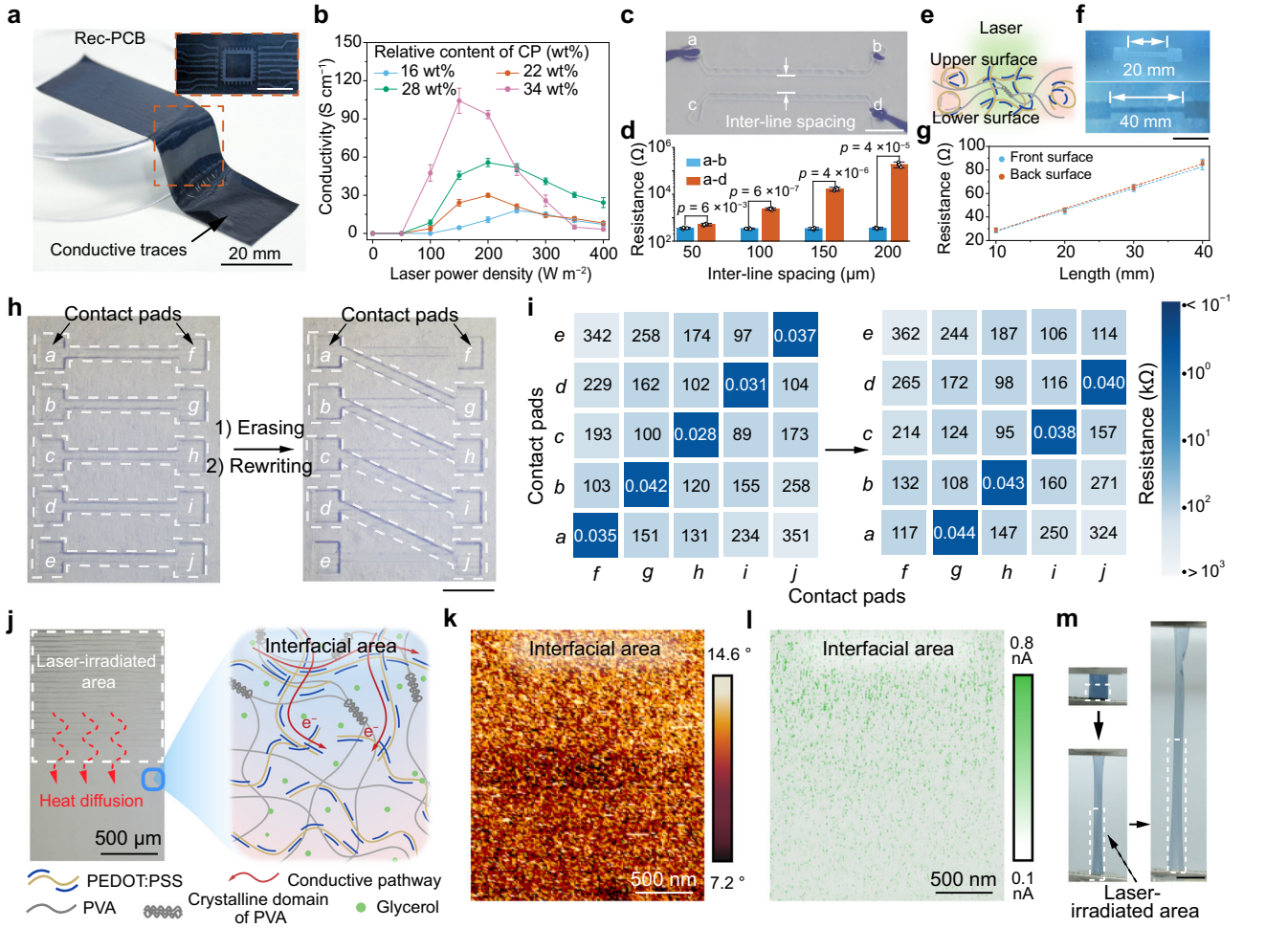

Fig. 4 | Micropatterning and reconfiguration of conductive traces. a Digital photograph of CP-PVA organogels (thickness: ~75 μm) with laser-defined conductive traces (scale bar in inset, 5 mm). **b** Conductivity of CP-PVA organogels with varied CP's contents after laser irradiation. **c, d** Cross-interference tests: the resistances between two contact pads (denoted as **a**–**d** in **c**) for conductive traces with different inter-line spacing (**d**). **e**–**g** Homogeneity tests: illustrative schematics showing the patterning of conductive traces within a CP-PVA organogels (**e**), digital photographs of conductive traces (scale bar, 20 mm) (**f**), and resistance of conductive traces with different lengths, measured at the upper and lower surfaces of CP-PVA organogels, respectively (**g**). **h**, **i** Reconfigurability tests: microscopic images of a conductive trace array (outlined with white dashed lines) fabricated within a CP-PVA organogel (scale bar, 100 μm) (**h**) and summary of resistance values measured between an arbitrary pair of contact pads (**i**). Interfaces between laser-irradiated and non-irradiated regions: microscopic photograph (**j**), AFM phase image (**k**), and tunneling current image recorded in TUNA mode (**l**). **m** Stretching behavior of a partially laser-irradiated CP-PVA organogel at a strain rate of 200% min^{-1} (scale bar, 15 mm). The areas outlined with white dashed lines represent laser-irradiated areas. The data in **b, d**, and **g** were presented as mean values ± standard deviation (s.d.), with four samples tested in independent measurements. Statistical significance was assessed using two-sided *t*-tests for comparisons between two groups (panel **d**), with significance determined by *p* values. Unless otherwise specified, CP-PVA organogels with a solid content of ~50 wt% (relative to the total mass of organogels) and CP's content of 22 wt% (relative to the total mass of CP and PVA) were used for the tests here.

environmental humidity level, demonstrating the high reliability and reproducibility of their electrical reconfigurability (Supplementary Fig. 57). As a whole, reversible control over the conductance of organogels was successfully achieved through nanophase structure engineering, leveraging the thermodynamically-driven reversible transformation of dynamic polymer networks in various ionic environments.

Reconfigurable printing circuit board with robust interfaces

With the highly dynamic characteristic of phase structure, the PVA-CP organogels provided an ideal platform for neuron-like bionic circuitry with remarkable reconfigurability at the hardware level, surpassing the limitations of previously reported intact conductive hydrogels or organogels. To showcase this unique feature, Rec-PCBs were fabricated by selectively annealing pristine CP-PVA organogels via laser irradiation, enabling the in-situ formation of patternable conductive domains through photothermal conversion (Fig. 4a).

To optimize the fabrication conditions, we first investigated the influence of the laser power on the conductivity and structural stability of CP-PVA organogels (Fig. 4b and Supplementary Fig. 58). With the laser power increasing (50-400 W m^{-2}), all the CP-PVA organogels with varied CP's and solid contents exhibited a similar conductivity trend: an initial increase with peak conductivities in a range of 4.5 S cm^{-1}–107.1 S cm^{-1} at a laser power of 150 W m^{-2} (corresponding to a local temperature of ~85 °C), followed by a decline at higher power. This reduction at relatively elevated power was likely due to the thermal-induced deswelling of organogels, as confirmed by infrared thermography (IRT) images and mechanical tensile tests, which showed localized overheating (*e.g.*,~200 °C for 250 W·m^{-2}) and deteriorated mechanical performance (Supplementary Figs. 58–60). Based

on these results, a laser power of 150 W m^{-2} was identified as an optimum condition for the patterning of conductive pathways, using CP-PVA organogels with a solid content of ~50 wt% (relative to the total mass of organogels) and CP's content of 22 wt% (relative to the total mass of CP and PVA) as the workpiece.

Upon laser irradiation, electrical circuits could be fabricated in situ within one CP-PVA organogel. The locally transformed conductive pathway, generated at a laser power of 150 W m^{-2}, exhibited a low optical contrast to the naked eye, but with boundaries visible under backlighting conditions due to the slight dehydration under irradiation (Supplementary Fig. 59). To quantitatively study the photothermal-induced formation of conductive pathways, CP-PVA organogels were subject to laser irradiation through a photomask. First, all the conductive traces with line widths ranging from 50 to 200 μm showed conductivities comparable to that of corresponding bulky materials, indicating the good size scalability of the laser-induced patterning (Supplementary Fig. 61). Second, the spatial resolution of the micropatterning process was evaluated by laser-writing pairs of adjacent conductive traces (Fig. 4c, d, and Supplementary Figs. 62, 63). Restrained by the inevitable thermal diffusion and resolution limit of the photomask used here, the minimum inter-line spacing between two conductive traces to avoid electrical cross-talk was determined to be 100 μm. Below this threshold, adjacent conductive traces became partially electrically connected. The resolution was expected to further improve by downsizing the laser spot through optical engineering in the future. Thirdly, the laser-induced conductive traces exhibited good uniformity and homogeneity in both horizontal and vertical directions: the absolute resistance of conductive traces followed Ohm's law as shown by a good linear relationship with the trace length (Fig. 4e–g), and exhibited good consistency for both the upper (directly exposed to laser) and lower surfaces (Supplementary Figs. 64 and 65).

Moreover, distinct from the conventional circuit with fixed trace layout determined fabrication, the CP-PVA organogels developed here possessed remarkable dynamic characteristics, enabled by the reconfigurable nanophase structure, resembling the adaptive nature of biological neuron networks. To showcase this characteristic, a Rec-PCB model with an array of dumbbell-shaped conductive traces was fabricated by selectively irradiating a CP-PVA organogel. The conductance between pairs of contact pads in the array (Fig. 4h and Supplementary Fig. 66) was measured and found to lie in line with the traces of laser irradiation, where the patterned traces exhibited conductance values up to 3–4 orders of magnitude higher than those of not-irradiated regions. Moreover, the conductive pathway could be erased by $CaCl_2$ treatment (followed by dialysis), resulting in a sharp resistance increase of 3–4 orders of magnitude. The pathways could then be rewritten through subsequent laser irradiation (Fig. 4i). This erasing-rewrite procedure could be repeated for more than 5 cycles, indicating the excellent reconfigurability (Supplementary Fig. 67).

In addition to enabling high reconfigurability, the in situ laser-assisted fabrication strategy also ensured the formation of a robust interface between the conductive traces and the surrounding matrix, attributed to the thermal gradient zone arising from inevitable heat diffusion within the organogels during irradiation (Fig. 4j). AFM analysis confirmed the presence of an interface layer between conductive and non-conductive domains. This layer facilitated remarkable interfacial adhesion and structural integrity through chain entanglement and non-covalent interactions (hydrogen bonds, π-π interactions, etc.) (Fig. 4k, l). The interfacial stability was successfully proved by tensile testing of CP-PVA organogels that were partially laser irradiated (Fig. 4m and Supplementary Fig. 68). The laser-patterned organogels showed mechanical performance comparable to that of pristine samples, with crack propagation formed upon strain commonly initiating at a random position rather than at the interface between irradiated and non-irradiated areas (Supplementary Video 1). Meanwhile, the patterned traces maintained stable electrical response under cyclic tensile strain, with no noticeable interfacial delamination (Supplementary Fig. 69). In contrast, most previously reported gel-based circuits lack in situ patternability and reconfigurability, and usually have to rely on adhesives for structural integrity.

Conformal soldering and closed-loop recycling

Beyond their electrical versatility, the high reconfigurability of CP-PVA organogels also enabled conformal soldering and closed-loop recyclability, advancing their utility in 3-dimensional (3D) and sustainable electronics. A widely used approach for the soldering of conductive gels involved a drying-reswelling procedure, where the conductive gels were dehydrated to achieve imitate contact with targeted substrates[17]. However, this strategy led to severe deformation or collapse of gels with complex 3D geometries. Herein, leveraging the high reconfigurability of the CP-PVA organogels, a geometry-preserving soldering strategy was developed to achieve strong and shape-retentive bonding between CP-PVA organogels and various substrates, without the need for complete dehydration.

In detail, for soldering, CP-PVA organogels at State III were coated with a thin layer of sans-glycerol CP/PVA aqueous solution (mass loading: 10 μL cm^{-2}), gently pressed against the targeted adherend (5 kPa), selectively dried overnight (for mechanical bonding), and then thermally annealed at 80 °C (for electrical connection). With this method, broken CP-PVA organogels could be healed together with no noticeable deterioration in mechanical and electrical performance (Fig. 5a–c). Importantly, complex geometries such as Möbius band structure could be preserved after soldering (Fig. 5d). In addition, CP-PVA organogels could also be strongly bonded to Cu, Sn, and Au substrates, achieving high adhesion toughness values of 1295, 1051, and 660 J m^{-2}, respectively (Fig. 5e–g and Supplementary Figs. 70–72). The electrical contacts between CP-PVA organogel and metals were proved to be ohmic contacts as indicated by the linear current-voltage response (Supplementary Fig. 73). Furthermore, the electrical contact could also be spatially patterned by leveraging local laser irradiation, where only the irradiated domains were electrically connected. This method allowed for a multichannel board-to-board connection between CP-PVA organogel and flexible PCB (Fig. 5h), a capability not easily achieved with previously reported adhesion strategies[23].

The mechanism underlying the wet soldering capability involved the solvent-mediated dynamic reconfiguration of the CP-PVA organogel network in the presence of the aqueous solder (sans-glycerol CP/PVA solution, Fig. 5i). Specifically, when aqueous CP/PVA solder was applied to the CP-PVA organogel at State III, the glycerol within the organogel and water from the solder underwent diffusion driven by a concentration gradient. On one hand, water infiltration partially loosened the original polymer network of organogels, resulting into a semi-interpenetrated network at the interface (Supplementary Figs. 74, 75a). Meanwhile, the glycerol in the organogels diffused into the aqueous solder and then induced the configuration transformation of CP (from solder) under thermal annealing (80 °C) or local laser irradiation, thus reducing the contact resistance between CP-PVA organogels and substrates (Supplementary Fig. 75b). This mechanism was further supported by control experiments using solders with different components, including PVA/CP glycerol solution, sans-glycerol CP aqueous solution, and sans-glycerol PVA aqueous solution, which was detailed in the Supporting Information (Supplementary Note 8, Supplementary Fig. 76).

In the closed-loop recycling, the CP-PVA organogels could be reprocessed in a closed-loop route, enabled by the highly dynamic organogel networks and the low volatility of glycerol. In detail, through dialysis with minimal water to remove glycerol (the glycerol-containing solution was retained for reuse), the CP-PVA organogels could be well dissolved in water by heating at 80 °C for 2 h (Fig. 5j). The resulting dispersion displayed excellent colloidal stability, with a zeta potential of −55 mV and uniform size distribution (295 nm), closing

https://doi.org/10.1038/s41467-025-68088-3

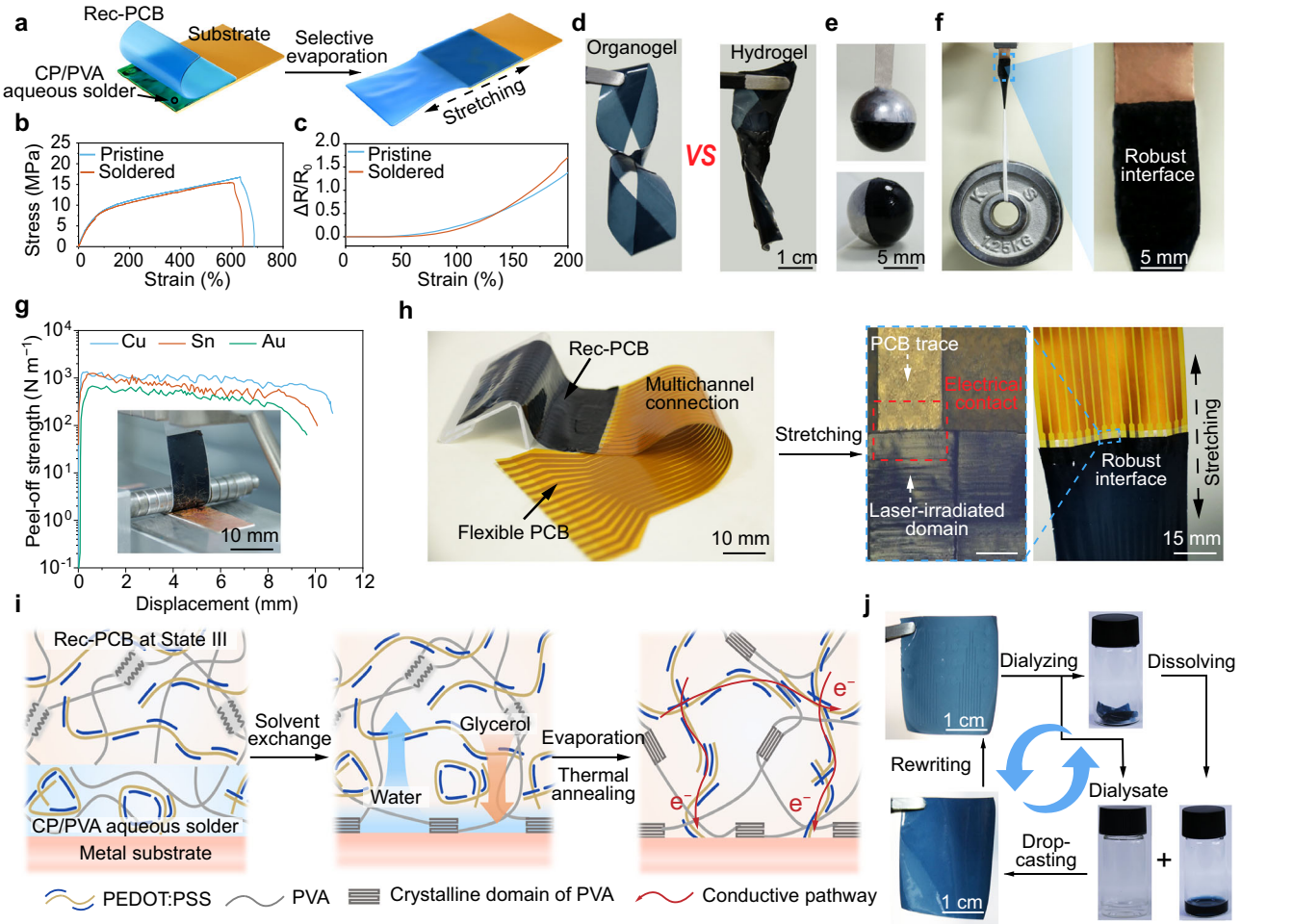

Fig. 5 | Conformal soldering and closed-loop recycling of reconfigurable conductive network. a Schematic of wet soldering process between CP-PVA organogel and various substrates. Stress-strain curves (**b**) and resistance change (**c**) of pristine CP-PVA organogel and soldered sample formed by soldering two CP-PVA organogel pieces. The tensile tests were performed at a strain rate of 200% min^{-1}. Demonstration of in situ conformal soldering. A Möbius-strip-shaped assembly was formed by soldering two CP-PVA organogel rings, whereas a hydrogel analog failed to retain structure during the soldering process (with the popular annealing-reswelling method) (**d**), CP-PVA organogel was also soldered to a stainless-steel hemisphere while preserving its hemispherical geometry (**e**). **f**, **g** Wet soldering of CP-PVA organogel to a Cu substrate (scale bar, 3 cm) (**f**) and 90° peel-off tests of CP-PVA organogels adhered onto Cu, Sn, and Au substrates (**g**). **h** Soldering of CP-PVA organogel to a flexible PCB. The CP-PVA organogels could be spatially patterned through laser irradiation, allowing for multichannel board-to-board connections. Scale bar of middle panel, 0.2 mm. **i** Schematic illustrating the mechanism of wet soldering. **j** Closed-loop recycling of CP-PVA organogels. Unless otherwise specified, CP-PVA organogels with a solid content of ~50 wt% (relative to the total mass of organogels) and CP's content of 22 wt% (relative to the total mass of CP and PVA) were used for the tests here.

matching the original (−50 mV, 255 nm; Supplementary Fig. 77). Subsequently, new organogels could be regenerated by re-introducing the recovered glycerol solution (obtained in the dialysis process), drop-casting, and selective evaporation at ambient environments. The regenerated organogels exhibited only mild reduction in mechanical performance and electrical properties (*e.g.*, 16.5 and 9.0% decreases in Young's modulus and toughness, respectively; Supplementary Fig. 78). In addition, the regenerated organogels also inherited excellent electrical reconfigurability, in which the conductive pathway could be erased via $CaCl_2$ treatment and then be re-constructed through laser irradiation (Supplementary Figs. 79 and 80).

Demonstrations

As a whole, by in situ tuning of the nanophase structure of conductive organogels through specific ion effect, three pairs of inherently conflicted properties were successfully integrated within one system: (*i*) high electrical and mechanical performance, (*ii*) patternability and reconfigurability of highly conductive pathways, and (*iii*) in situ solderability and closed-loop recyclability of conductive gels. To showcase these capabilities, four representative applications were developed, including (*i*) organogel-based printing circuit boards (PCBs) for plug-and-play interconnection with conventional rigid PCBs, (*ii*) organogel-based integrated electronic wrist bands for electrophysiological signal capture, (*iii*) in situ rewritable electroluminescent devices and rewritable LED bands, and (*iv*) organogel-based stretchable circuitry models for audio playing.

As a first example, a 6-channel organogel-based PCB was fabricated (line spacing: 5.5 mm, line width: 1 mm) (Fig. 6a). The PCB was soft, stretchable, and could be connected to conventional rigid PCBs through zero-insertion-force (ZIF) connectors for analog signal transmission (Fig. 6b). Attributed to the high structural integrity with high toughness, the electrical connection/disconnection of organogel-based PCB to the conventional rigid PCB could be repeated for >1000 cycles, with no noticeable deterioration in electrical performance (Supplementary Fig. 81). Moreover, the organogel-based PCB demonstrated a broader operational frequency range compared to its hydrogel counterpart, probably due to the lower relative permittivity of the organic system (Supplementary Fig. 82).

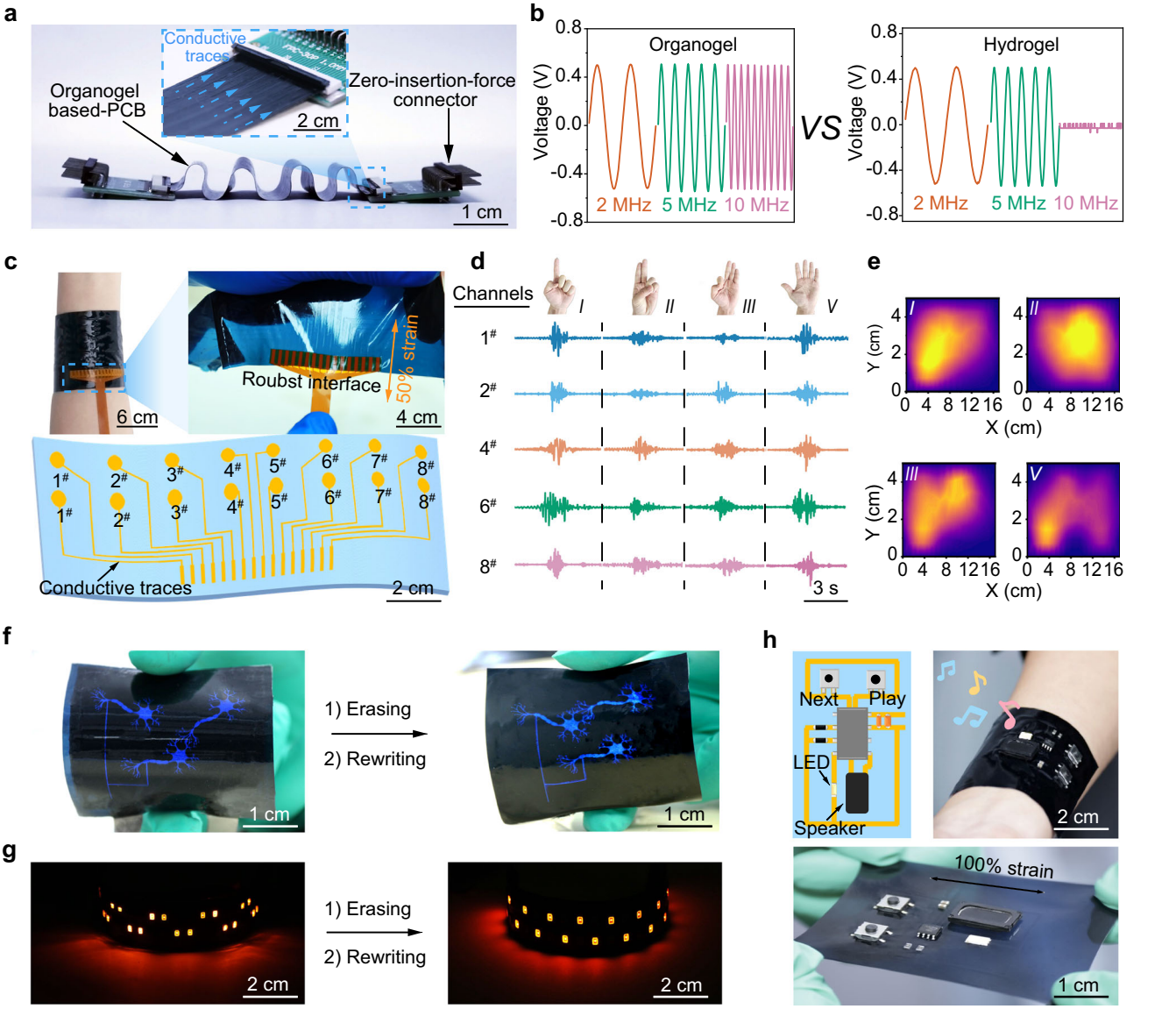

Fig. 6 | Demonstrations of reconfigurable electronics. a, **b** Digital photograph and analog signal transmission of 6-channeled organogel-based or hydrogel-based PCBs connected to conventional rigid PCBs through ZIF connectors. **c** Digital photograph of CP-PVA organogel-based digital wristband containing 8 pairs of electrodes for electrophysiological signal recording. sEMG signals recorded with the organogel-based digital wristband during the performance of four different gestures (gestures I, II, III, V) (**d**); sEMG maps corresponding to the four-hand gestures were generated by calculating the root mean square (RMS) amplitude for each channel (**e**). Digital photograph of reconfigurable organogel-based EL devices (**f**) and LED bands (**g**): The EL devices and the LED bands were powered by an alternating current voltage of 100 V at 1 kHz and a direct current of 20 mA, respectively. **h** Digital photograph of a stretchable circuitry model based on an organogel PCB for audio playing, consisting of resistors, capacitors, switches, an LED, a speaker, and an FLM038A integrated circuit (IC). The audio player circuitry model was highly soft and operable upon strain. Unless otherwise specified, CP-PVA organogels with a solid content of ~50 wt% (relative to the total mass of organogels) and CP's content of 22 wt% (relative to the total mass of CP and PVA) were used for the experiments here.

Secondly, a CP-PVA organogel-based digital wristband in situ patterned with 8 pairs of electrodes was prepared for electrophysiological signal recording (Fig. 6c). In detail, the good biocompatibility of CP-PVA organogels was a prerequisite for high-quality signal acquisition, which was confirmed by both in vitro cytocompatibility tests and in vivo subcutaneous implantation assessment (Supplementary Note 9, Supplementary Fig. 83)[31,32]. Furthermore, compared to the previously reported bioelectrodes, the digital wristband showed low electrical impedance and robust structural integrity while maintaining a stable electrical connection when interfaced with a signal recorder via a PCB through a conformal soldering method as described above (Fig. 6c, Supplementary Figs. 84, 85)[33]. Particularly, the overall impedance and phase angle of the digital wristband exhibited negligible changes under 50% tensile stretching, demonstrating the excellent reliability of the system (Supplementary Fig. 86). Consequently, high signal-to-noise ratio electrophysiological recordings were achieved, surpassing those obtained with commercially available electrodes (Supplementary Fig. 87). As an example, real-time monitoring of muscle activity was demonstrated by recording the surface electromyography (sEMG) maps in space and time domains, highlighting potential applications in medical diagnosis or human-machine interaction (Fig. 6d, e, Supplementary Fig. 88 and Supplementary Video 2). At last, the CP-PVA organogel-based digital wristband demonstrated excellent environmental stability, maintaining a high signal-to-noise ratio (~21 dB) and reliable sEMG recording performance even after one week of

exposure to ~20% and ~70% relative humidity conditions (Supplementary Fig. 89).

Thirdly, to showcase the reconfigurability, organogel-based electroluminescence (EL) devices and rewritable LED bands were prepared (Fig. 6f, g, Supplementary Figs. 90, 91). The EL devices consisted of a laser-patterned PVA-CP bottom electrode, polydimethylsiloxane (PDMS)-ZnS EL layer, and Cu top electrodes. Upon electric power, the EL emission accurately replicated the layout of the electrical traces patterned within the CP-PVA organogels. More importantly, the layout could be dynamically altered by in situ rewriting the conductive traces through sequential treatment with $CaCl_2$ solution, dialysis, and laser scribing (Fig. 6f, Supplementary Figs. 92, 93, and Supplementary Video 3). The reconfigurable LED band featured an LED matrix soldered onto the CP-PVA organogel substrate using PVA/CP aqueous solder. Its conductive pathways could be adjusted by leveraging the electrical reconfigurability of CP-PVA organogel, enabling on-demand modification of the electrical layout (Fig. 6g, Supplementary Fig. 91). Notably, beyond these examples, the hardware-level reconfigurability is expected to inspire the design of next-generation biomimetic electronics for a variety of applications, including tissue engineering, information processing, and cyborgs. For example, dynamically reconfigurable conductive organogels could support neural tissue culture with spatiotemporal plasticity.

Finally, to demonstrate the excellent solderability of the CP-PVA organogels for use as printing circuit boards, a functional stretchable audio-playing circuit was assembled. The circuit comprised resistors, capacitors, switches, an LED, a speaker, and an FLM038A integrated circuit (IC) (Fig. 6h, Supplementary Fig. 94, Supplementary Table 7). The electronic components were soldered onto a laser-patterned organogel-based PCB using CP/PVA aqueous solder followed by thermal annealing, resulting in strong bonding and reliable electrical connectivity. The final circuit was highly soft, stretchable, and capable of playing preloaded audio tracks stored in the FLM038A chip during operation (Supplementary Video 4). At last, given the ion-specific mechanism that underlies the organogel's phase reconfigurability, the CP-PVA organogel-based circuit board was expected to be sensitive to ions, especially kosmotropic cations. A potential strategy to mitigate this issue involves encapsulating the organogels with detachable ion-selective barrier materials after fabrication, which will be explored in future studies.

Discussion

This work presents a general strategy for constructing neuron-imitating reconfigurable generation electronics by leveraging reversible nanophase regulation of dynamic non-covalent conductive networks. Specifically, the nanophase structure of the non-covalent conductive networks exhibits significant response to specific ions, governed by thermodynamics, allowing for reversible modulation of both electrical and mechanical properties. As a result, the organogel-based conductive networks could successfully integrate high electrical performance with several additional features that are typically challenging to combine: mechanical performance, conductance reconfigurability, in situ patternability of conductive pathways, in situ solderability with spatial resolution, and closed-loop recyclability.

With these unique features, neuron-tissue-like reconfigurable printing circuit boards can be designed and utilized for the application of reconfigurable bioelectronics and sustainable electronics. Moreover, the integration of in situ patterning of conductive traces and soldering capability successfully addressed a long-standing challenge in gel-based bioelectronics: achieving robust, multichannel interconnection between gel systems and conventional rigid electronics (such as IC and PCB). A reliable board-to-board connection between CP-PVA organogel and commercial flexible PCB is demonstrated here, a capability not easily realized using conventional adhesion strategies for conductive gels.

At last, this study greatly deepens the fundamental understanding of the evolution of the nanophase microstructure of conductive gel and, more essentially, elucidates the underlying mechanism of ion-driven modulation. The conceptual framework introduced here is expected to inspire the development of reconfigurable bionic devices and help bridge the interface among the biological world, aqueous gel electronics, and conventional rigid electronics.

Methods

Materials

Poly(3,4-ethylenedioxythiophene):polystyrene sulfonate was ordered from Heraeus Epurio Ltd (Grade PH 1000) or Sigma-Aldrich (Orgacon™ ICP 1050), or prepared following the method described below. Glycerin (AR, 99%), Acrylamide (AR, 99%), ammonium persulphate (APS, AR, 98%), methacrylic anhydride were (94%, Contains 2% stabilizer), triethylamine (AR, 99%), and α-Ketoglutaric acid (98%) were supported by Haohong Pharmaceutical Co., Ltd. (Shanghai, China). Poly(vinyl alcohol (PVA, Mw:89000–98000, 99% alcoholysis), aniline (AR, 99%), silver powder (Ag, 5 μm), sodium chloride (NaCl, 98%), potassium chloride (KCl, 98%), cesium chloride (CsCl, 98%), lithium chloride (LiCl, 98%), calcium chloride ($CaCl_2$, 98%), sodium sulfate (Na_2SO_4, 98%), sodium carbonate (Na_2CO_3, 98%), sodium citrate (98%), sodium iodide (NaI, 98%), acetone (98%), ethanol (98%), hydrochloric acid (HCl, analytical reagent grade), and dimethyl sulfoxide (DMSO) were purchased from Shanghai Aladdin Biochemical Technology Co., Ltd.

Synthesis of PEDOT:PSS with varying PSS contents

PEDOT:PSS was synthesized via oxidative polymerization of 3,4-ethylenedioxythiophene (EDOT) in the presence of sodium polystyrene sulfonate (NaPSS, Mw: ~20 kDa). Briefly, EDOT monomer (50 μL, 47 mmol) was dispersed in 15 mL of NaPSS aqueous solution under vigorous stirring at room temperature, with the molar ratio of EDOT to the sulfonate units of NaPSS adjusted to be 1:3, 1:4, or 1:5. The mixture was stirred for 30 min to ensure uniform dispersion and effective interaction between EDOT and NaPSS. Subsequently, anhydrous ferric chloride ($FeCl_3$, 15.3 mg) and sodium persulfate (130 mg, 55 mmol) were added, and the reaction was allowed to proceed under continuous stirring for 12 h. During this period, the solution gradually turned dark blue, confirming the formation of PEDOT:PSS. Finally, the resulting dispersion was purified using cation- and anion-exchange resin to remove residual salts.

Preparation of CP-PVA organogels

Typically, unless otherwise specified, PEDOT:PSS aqueous solutions with the grade of PH 1000 from Heraeus Epurio Ltd were used for the preparation of CP-PVA organogels. This PEDOT:PSS grade was one of the most widely used formulations in the research community, attributed to its high conductivity and excellent processability. The pristine PEDOT:PSS aqueous solutions were first filtered through a syringe filter with a pore size of 0.45 μm to remove large particles and then added to a PVA glycerol solution (the content of glycerol was 4 wt % relative to the total mass of final solution, and the concentrations of CP and PVA were 7.4 mg mL^{-1} and 26.1 mg mL^{-1} respectively, if not particularly mentioned). The obtained suspension was drop-casted on a glass plate (volumetric loading: 0.1 mL cm^{-2}) and dried at the ambient environment (~25 °C) overnight to obtain free-standing p-CP-PVA organogels with a thickness of ~92 μm. The solid contents of p-CP-PVA organogels could be controlled by varying the glycerol's relative contents in the precursor solutions. The p-CP-PVA organogel exhibited a high resistance. To improve the conductance, a dry annealing process was implemented at 80 °C for 2 h at ambient conditions with relative humidity (RH) of 40–60%.

For the preparation of a thin CP-PVA organogel film with high optical transparency, a spin-coating method was employed, where the precursor glycerol solutions containing CP and PVA were spin-coated

onto glass plates or elastomer films (EcoflexTM 00-45 Near Clear™) previously treated by oxygen plasma at speeds of 500, 700, 900, 1100, 1300, and 1500 rpm. At last, conductive organogel film was obtained by drying at the ambient environment (~25 °C) overnight and an annealing process at 80 °C for 2 h.

In the control experiments, four types of samples were prepared, including CP-PVA organogels based on other organic solvents, CP-PVA hydrogel, pure CP, and PVA organogels. (*i*) CP-PVA organogels based on other organic solvents: different solvents (DMF, DMSO, ethylene glycol, and polyglycerol, respectively) were added into the CP-PVA mixture solution (mass ratio of CP to PVA = 22:78), and organogels were obtained following a similar procedure as described above. (*ii*) CP-PVA hydrogels: CP-PVA organogels were dialyzed in water, dried at the ambient environment (25 °C, ~50 % relative humidity), and then reswollen in deionized water to yield CP-PVA hydrogels. (*iii*) Pure CP organogels: PEDOT:PSS suspensions were added with glycerol (4 wt%, relative to the total mass of solution), and then drop-casted onto glass plates previously treated with O_2 plasma for 5 min (volumetric loading: 75 μL cm^{-2}), followed by annealing at 80 °C for 2 h. (*iv*) Pure PVA organogels: PVA glycerol suspensions containing 4 wt% glycerol and 10 wt% PVA were drop-casted onto glass plates previously treated with O_2 plasma for 5 min (volumetric loading: 30 μL cm^{-2}), and dry annealed at 80 °C for 2 h.

Preparation of methacrylate PVA (PVA_{MA}) and CP-PVA_{MA} organogels

The PVA_{MA} was synthesized by the esterification reaction between PVA and methacrylic anhydride, following the previous literarure[34]. First, PVA (Sigma-Aldrich, 89000–98000 kDa, 98% hydrolyzed) was dissolved in water by heating at 90 °C for 2 h to obtain a 10 wt% PVA solution. Then, the PVA solution was added with methacrylic anhydride (5 mol% relative to PVA) under stirring, left to react at 60 °C for 48 h, and then quenched by neutralizing with triethylamine. At last, PVA_{MA} power was obtained by slowly dropping the reaction solution into acetone (5 equivalent volumes relative to the solution) under vigorous agitation, filtering, washing with excessive acetone, and drying at 60 °C.

For the preparation of the CP-PVA_{MA} organogels, glycerol suspensions (4 wt%, relative to the total mass of solution) containing 7.4 mg mL^{-1} of CP, 0.3 mg mL^{-1} of α-ketoglutaric acid, and 26.1 mg mL^{-1} of PVA_{MA} (CP's relative content: 22 wt%) was dropped-casting on a glass plate (volumetric loading: 0.1 mL cm^{-2}), and dried under ambient conditions (25 °C) for 24 h to selectively evaporate most of the water. At last, a free-standing CP-PVA_{MA} organogel was successfully obtained and crosslinked by exposure to ultraviolet (UV) light (wavelength: 365 nm) for 30 min. For the preparation of CP-PVA_{MA} organogels without chemical crosslinking, a polymerization inhibitor was added to a sans-photoinitiator glycerol solution (4 wt%, relative to the total mass of solution) containing 7.4 mg mL^{-1} of CP and 26.1 mg mL^{-1} of PVA_{MA} (CP's relative content: 22 wt%, relative to the total mass of PVA and CP), and then followed with a similar procedure as described above except without UV exposure step.

Preparation of polyaniline (PANi)-PVA and Ag-PVA organogels

PANi-PVA organogels were synthesized following an ice-templated polymerization method reported previously[35]. In detail, a monomer-containing solution (solution A) was first prepared by adding 80 μL of HCl solution (35 wt%) and 28 mg of aniline in 1 mL of 10 wt% PVA solution, followed by vigorous stirring until a clear and transparent solution was formed. The mixture solution was cooled in an ice bath. Subsequently, 0.5 mL of ammonium persulfate (APS) solution (162 mg mL^{-1}) was added to solution A. The resulting solution was poured into a mold and frozen in liquid nitrogen for 2 h. Finally, the frozen samples were transferred to a refrigerator at −20 °C and kept static for 24 h, during which aniline was polymerized to form PANi. PANi-PVA organogels were obtained by thawing the frozen samples at room temperature, followed by dialysis in 50 wt% glycerol solution for 12 h and drying at ambient temperature for 24 h.

For the preparation of the Ag-PVA organogels, 0.15 g of silver flake powder (diameter: 5 μm) and 0.6 mL of a glycerol solution (50 wt%) were added to 2 mL of a 10 wt% PVA solution and mixed with a planetary-type mixer at 2500 rpm for 10 min (HMV200D, Shenzheng Hasai Technology, China). Then, the mixture solution was drop-casted onto a glass plate (volumetric loading: 0.1 mL cm^{-2}) and dried at ambient temperature (~25 °C) for 24 h.

Preparation of CP-PAM organogels and CP-PNIPAm organogels

PAM was first synthesized by free radical polymerization in aqueous solution. Specifically, 1.0 g of acrylamide monomer was dissolved in 10 mL of deionized water to obtain a clear 10 wt% solution. Ammonium persulfate (APS, 10 mg, corresponding to 1 wt% of acrylamide) was then introduced as the radical initiator, followed by the addition of tetramethylethylenediamine (TEMED, 5 μL, ~0.5 wt%) as the accelerator. The solution was purged with nitrogen for 20 min to remove dissolved oxygen, sealed, and allowed to polymerize at ambient temperature (25 °C) under gentle stirring for 4 h. The viscous product was dialyzed against deionized water for 48 h to remove unreacted monomers and initiators, and subsequently freeze-dried to obtain linear PAM in the form of a white powder. For CP-PAM organogel preparation, pristine PEDOT:PSS aqueous solution was first passed through a 0.45 μm syringe filter to remove large particles. The filtered PEDOT:PSS was then mixed with a PAM–glycerol solution, in which glycerol accounted for 4 wt% of the total solution, while the concentrations of CP and PAM were maintained at 7.4 mg mL^{-1} and 26.1 mg mL^{-1}, respectively (unless otherwise specified). The resulting suspension was drop-cast onto a glass plate with a volumetric loading of 0.1 mL cm^{-2} and dried overnight at ambient conditions (~25 °C) to yield free-standing p-CP-PAM organogels. The as-prepared organogels initially exhibited high resistance, which was subsequently reduced by subjecting the samples to a thermal annealing treatment at 80 °C for 2 h to improve their electrical conductivity. CP-PNIPAm organogels were synthesized using a similar procedure, with PNIPAm replacing PAM as the polymer matrix.

Transitioning of CP-PVA organogels among different conductance states

Unless otherwise specified, the CP-PVA organogels used in the tests had a solid content of ~50 wt% (relative to the total mass of organogel) and a CP fraction of 22 wt% (relative to the total mass of CP and PVA). (*i*) The thermally-annealed CP-PVA organogels were donated as State I. (*ii*) To obtain State II, the CP-PVA organogels in State I were soaked with a glycerol solution containing 2 mol L^{-1} $CaCl_2$ for 3 days, followed by selective evaporation at an ambient environment (~25 °C, RH: 40–60%) for 24 h. (*iii*) To obtain State III, the CP-PVA organogels at State II were dialyzed in a 15 wt% glycerol solution for 24 h and partially dried in an ambient environment for 24 h. (*iv*) To obtain State I_2, the CP-PVA organogels at State III were thermal annealed at 80 °C for 2 h under ambient conditions (~25 °C, RH: 40–60%).

To pattern the conductive traces, the p-CP-PVA organogels or CP-PVA organogels at State III were irradiated by a continuous laser (DT1-3W; Lighthouse Photonics, China) with an optical power density of 150 W m^{-2} (wavelength: 532 nm, spot size: 0.3 mm) at a fixed scanning speed of 6 cm s^{-1}, if not mentioned. An infrared thermal imager (A615, Teledyne FLIR, U.S.) was employed to record the temperature variations and infrared thermal images of the CP-PVA organogels during laser irradiation, capturing their photothermal response. To obtain fine conductive traces, CP-PVA organogels at State III were subject to laser irradiation through a photomask. The pre-patterned photomask was brought into intimate contact with the organogel surface and precisely aligned under microscopic observation (the design of the

photomask is shown in Supplementary Figs. 61, 65). Laser irradiation was subsequently applied through the photomask apertures to induce conductive traces. To erase the conductance of the CP-PVA organogels, the $CaCl_2$ treatment and dialysis were performed, following the protocol described above.

Determination of water and glycerol contents in organogels

The solid content of CP-PVA organogel was obtained by measuring the total mass (m_t) of wet samples and dry mass (m_s) after complete drying. To determine the glycrol contents, the dispersion medium of organogel was extracted by dialysis in a defined amount of deionized water (2 mL) and filtered through a membrane with a pore size of 0.22 µm prior to high-performance liquid chromatography (HPLC) analysis. The measurements were performed on an HPLC system (Waters e2695, Waters Corporation, US) equipped with a refractive index detector and an Aminex HPX-87H column (300 mm × 7.8 mm, 9 µm). The column temperature was set as 35 °C, and 5 mmol L^{-1} H_2SO_4 was used as the mobile phase at a flow rate of 0.6 mL min^{-1}. Standard glycerol solutions (0.02–1.0 mg mL^{-1}) were freshly prepared to construct an external calibration curve (linear correlation coefficient, $R^2 \geq 0.999$). The mass fractions of glycerol (F_g) and water (F_w) in the CP-PVA organogel were calculated using Eq. (1) and Eq. (2), respectively.

$$F_{\mathrm{g}} = \frac{C_{\mathrm{gly}} \times 2\,\mathrm{mL}}{m_{\mathrm{t}}} \times 100\% \tag{1}$$

$$F_{\mathrm{w}} = \left(\frac{m_{\mathrm{t}} - m_{\mathrm{s}}}{m_{\mathrm{t}}} - F_{\mathrm{g}}\right) \times 100\% \tag{2}$$

where C_{gly} is the concentration determined from the calibration curve.

Conformal soldering of conductive organogels and measurement of contact resistance

The CP-PVA organogels could be soldered to themselves or some common metals such as Cu, Sn, and Au. Typically, CP-PVA organogel was first dip-coated with a sans-glycerol CP/PVA aqueous solution (containing 26.1 mg mL^{-1} PVA and 7.4 mg mL^{-1} CP) and then gently pressed against the targeted adherend (~5 kPa), and left to stand at an ambient temperature (~25 °C) for 12 h. Afterward, the assembly was thermally annealed at 80 °C for 2 h or subjected to via local laser irradiation to establish an electrical connection. Particularly, for bonding with metal substrates, the surface was first cleaned with ethanol to remove organic contaminants, followed by 5 min of oxygen plasma treatment to enhance surface hydrophilicity.

In the control experiments, different soldering solutions were employed including PVA/CP glycerol solution (glycerol content: 4 wt% relative to the total mass of the final solution, CP and PVA concentrations: 7.4 mg mL^{-1} and 26.1 mg mL^{-1} respectively), sans-glycerol aqueous CP solution (solid content: 1.1–1.3 wt%), and sans-glycerol aqueous PVA solution (solid content: ~10 wt%). The soldering process was then performed following the same procedures as described above.

The contact resistances between the organogel and conductive adherent were measured using a source meter (2450 Graphical Source Meter, Keithley, U.S.) in a two-probe configuration. A linear voltage sweeps from −3 V to +3 V were applied, and the corresponding current response was recorded.

Fabrication of organogel-based printing circuit boards

The CP-PVA organogels, with a solid content of ~50 wt% and CP's relative content of 22 wt% (relative to the total mass of CP and PVA), were used for experiments. The CP-PVA organogels were cut into rectangular strips measuring 10 cm in length and 3.5 cm in width using a scalpel. Subsequently, 6 channels conductive traces (spacing: 5.5 mm, width: 1 mm) were induced on the CP-PVA organogels via continuous laser direct writing with an optical power density of 150 W m^{-2} (wavelength: 532 nm, spot size: 0.3 mm) at a fixed scanning speed of 6 cm s^{-1}. The organogel-based printing circuit traces could be connected to two zero-insertion-force (ZIF) connectors, capable of transmitting analog signals within a wide range of frequencies (10 MHz-100 HZ).

Closed-loop recycling of conductive CP-PVA organogels

CP-PVA organogels can be closed-loop recycled through dissolution followed by selective solvent evaporation. Specifically, CP-PVA organogels (30 mm in length and 20 mm in width) with laser-patterned conductive traces were dialyzed in a small amount of water to remove glycerol, and the resulting dialysis solution containing glycerol was collected for subsequent reuse. The dialyzed sample was then dispersed in 1 mL of deionized water and stirred at 80 °C until a clear solution was obtained. After cooling to room temperature, the previously collected dialysis solution was added to recover the glycerol content (2 wt%, relative to the total mass of the solution). The resulting mixture was filtered through a 220 µm pore size membrane, drop-cast onto a glass plate (volumetric loading: 0.2 mL cm^{-2}), and allowed to dry under ambient conditions (25 °C) for 24 h.

Preparation of organogel-based electronic wristband and EMG signal capture

A p-CP-PVA organogel (180 mm × 50 mm × 75 µm) was patterned into electrical traces by a continuous laser (150 W m^{-2}, wavelength: 532 nm, spot size: 0.3 mm, speed: 6 cm min^{-1}) to fabricate a one-body digital wristband. The resulting digital wristband was connected to a biosignal acquisition board (Cyton Board, OpenBCI, U.S.) via a flexible printed circuit board (FPCB) for EMG recording. The electrical connection between the wristband and the FPCB was achieved using the conformal soldering method described above, where an aqueous CP/PVA solder was applied at the interface and selectively irradiated by laser (Fig. 6c). The acquired signals were wirelessly transmitted to a computer via Bluetooth and post-processed with band-pass (0.5–100 Hz) and notch (50/60 Hz) filters.

Fabrication of in-situ rewritable electroluminescence devices

Organogel-based electroluminescence devices adopted a sandwich structure[36], consisting of a patterned organogel bottom electrode, an electroluminescent layer, an insulating layer, and a Cu top electrode (Supplement Fig. 88). Patterned p-CP-PVA organogels (solid content: 40 wt%, relative to the total mass of organogels, CP content: 22 wt% relative to the total mass of CP and PVA), serving as the bottom electrode, were prepared through laser irradiation as described above. The patterned p-CP-PVA organogels were then coated with a ZnS electroluminescent layer through blade-coating uncured PDMS precursor containing ZnS particles (mass ratio of PDMS to ZnS = 1:1.4) and solidifying in the ambient environment (25 °C) for 4 h. Next, barium powder was dispersed in uncured PDMS at a 1:1 mass ratio and applied atop the light-emitting layer to serve as the insulating layer, followed by curing in the ambient environment for 2 h. Finally, conductive copper paste was applied to the surface of the insulating layer to form the electrode layer. The EL devices were activated by applying an alternating current of 100 V and 3 kHz between the CP-PVA organogel and the conductive copper electrodes.

To reconfigure the electroluminescent pattern, a 15 wt% glycerol solution containing 2 M $CaCl_2$ solution was dropped onto the surface of the bottom electrodes in the EL devices and left static for 3 days, during which the previously patterned conductive traces were erased (Supplementary Fig. 90, 91). Then, $CaCl_2$ was removed by repeated dialysis in a 15 wt% glycerol solution (four times), followed by partial drying in the ambient environment. The recovered high-resistance organogel electrode was subsequently repatterned with new

conductive traces via continuous laser direct writing, enabling the rewriting of the electroluminescent pattern.

Fabrication of in-situ rewritable LED bands

The p-CP-PVA organogels, with a solid content of ~40 wt% and CP's relative content of 22 wt% (relative to the total mass of CP and PVA), were used for experiments. Subsequently, conductive traces were patterned on the CP-PVA organogel by a continuous wave laser (power density: 150 W m^{-2}, wavelength: 532 nm, spot size: 0.3 mm, speed: 6 cm min^{-1}). The conductive traces as shown in Supplementary Fig. 53. The aqueous CP/PVA solder (the concentrations of CP and PVA were 7.4 mg mL^{-1} of CP and 26.1 mg mL^{-1}) was printed onto the CP-PVA organogel through a customized stencil, serving as contact pads for LEDs. Then, the LEDs are placed on the corresponding contact pads. Finally, the LED bands were left at ambient temperature (~25 °C) to selectively evaporate excess water from the CP/PVA aqueous solder, and powered by a constant current of 20 mA.

To study the in situ re-writability of CP-PVA organogel-based LED bands. CP-PVA organogel-based LED bands were immersed in 15 wt% glycerol solutions (relative to the total mass of solution) with a salting-in effect (e.g., 2 M $CaCl_2$ solution) for 3 days. Then, the LED bands were dialyzed in 15 wt% glycerol solution for 24 h and selectively evaporated in an ambient environment (~25 °C) overnight to erase the conductive traces of CP-PVA organogels. The CP-PVA organogels were subsequently rewritten with new conductive traces via continuous laser direct writing with an optical power density of 150 W m^{-2} (wavelength: 532 nm, spot size: 0.3 mm) at a fixed scanning speed of 6 cm s^{-1} (Supplementary Fig. 53).

Fabrication of organogel-based stretchable circuitry model for audio playing

The organogel-based stretchable circuitry model was fabricated by constructing an audio circuit with a patterned CP-PVA organogel serving as a printing circuit board. Here, we patterned the p-CP-PVA organogels to create conductive traces and contacts for circuit applications. The p-CP-PVA organogels, with a solid content of ~40 wt% and CP's relative content of 22 wt% (relative to the total mass of CP and PVA), were used for experiments. Subsequently, conductive traces were constructed on the p-CP-PVA organogels by a continuous wave laser (power density: 150 W m^{-2}, wavelength: 532 nm, spot size: 0.3 mm, speed: 6 cm min^{-1}). The CP/PVA aqueous solder (the concentrations of CP and PVA were 7.4 mg mL^{-1} of CP and 26.1 mg mL^{-1}) was printed onto the p-CP-PVA organogel, serving as contact pads for electronic components. The electronic components are placed on the corresponding contact pads. Finally, the electronic components were left at room temperature to allow the evaporation of excess water from the CP/PVA aqueous solder. Detailed circuit diagram and printed circuit board design are provided in Supplementary Fig. 54, and the list of components can be found in Supplementary Table 5. The organogel-based audio player circuit was powered by a lithium-ion battery.

Statistical analysis

All experiments were conducted with a sample size of at least four ($n \geq 3$), and results were presented as mean ± standard deviations (SD) or as box-and-whisker plots. Statistical analyses were performed using the two-sided *t*-test for comparisons between two groups or one-way analysis of variances (ANOVA) for comparison among multiple groups, using Origin software. Significance levels were assessed using *p* values. For AFM characterizations shown in Figs. 2k, 3g, and 4j–l, the displayed images correspond to one of the repeated trials, and the reproducibility across independent replicates was confirmed. Electrophysiological recording data were pre-processed using a bandpass filter (5–50 Hz) implemented in Origin software. All statistical analyses were performed using IBM SPSS Statistics 27.

Ethical approval

All animal experiments were performed in accordance with the Guide for the Care and Use of Laboratory Animals and were approved by the Institutional Animal Care and Use Committee (IACUC) of Nanjing University of Science and Technology (authorization number: ACUC-NUST-20250228019).

Surface electromyography recordings were performed on healthy adult male volunteers (22-28 years old) after written informed consent was provided. According to the Human Research Ethics Committee (HRECs) of Nanjing University of Science and Technology, formal ethical approval for these surface electromyography recordings was not required.

Reporting summary

Further information on research design is available in the Nature Portfolio Reporting Summary linked to this article.

Data availability

The main data supporting the results in this study are available within the paper and its Supplementary Information. Source data are provided with this paper.

References

1. Wang, M. et al. Printable molecule-selective core-shell nanoparticles for wearable and implantable sensing. *Nat. Mater.* **24**, 589–598 (2025).
2. Xie, R. et al. A movable long-term implantable soft microfibre for dynamic bioelectronics. *Nature* **645**, 648–655 (2025).
3. Gautham, V. et al. Slip-actuated bionic tactile sensing system with dynamic DC generator integrated E-textile for dexterous robotic manipulation. *Nat. Commun.* **16**, 7005 (2025).
4. Chen, S. et al. Artificial organic afferent nerves enable closed-loop tactile feedback for intelligent robot. *Nat. Commun.* **15**, 7056 (2024).
5. Homberger, D. G. & de Silva, K. N. The role of mechanical forces on the patterning of the avian feather-bearing skin: a biomechanical analysis of the integumentary musculature in birds. *J. Exp. Zool. B Mol. Dev. Evol.* **298**, 123–139 (2003).
6. Hütt, M. T., Kaiser, M. & Hilgetag, C. C. Perspective: network-guided pattern formation of neural dynamics. *Philos. Trans. R. Soc. B Biol. Sci.* **369**, 25180302 (2014).
7. Zhong, W. et al. Spatiotemporally responsive hydrogel dressing with self-adaptive antibacterial activity and cell compatibility for wound sealing and healing. *Adv. Healthc. Mater.* **12**, e2203241 (2023).
8. Marder, E. Neuromodulation of neuronal circuits: back to the future. *Neuron* **76**, 1–11 (2012).
9. Bargmann, C. I. Beyond the connectome: how neuromodulators shape neural circuits. *Bioessays* **34**, 458–465 (2012).
10. Mazlouman, S. J., Jiang, X. J., Mahanfar, A., Menon, C. & Vaughan, R. G. A reconfigurable patch antenna using liquid metal embedded in a silicone substrate. *IEEE Trans. Antennas Propag.* **59**, 4406–4412 (2011).
11. Fink, Z. et al. Repairable and reconfigurable structured liquid circuits. *Adv. Funct. Mater.* **34**, 2402708 (2024).
12. Park, J. E. et al. Rewritable, printable conducting liquid metal hydrogel. *ACS Nano* **13**, 9122–9130 (2019).
13. Liu, Y. et al. Rewritable electrically controllable liquid crystal actuators. *Adv. Funct. Mater.* **33**, 2302110 (2023).
14. Zhao, Y. et al. Somatosensory actuator based on stretchable conductive photothermally responsive hydrogel. *Sci. Robot.* **6**, eabd5483 (2021).
15. Lin, Y. L. et al. Light-responsive MXenegel via interfacial host-guest supramolecular bridging. *Nat. Commun.* **15**, 916 (2024).

16. Doshi, S. et al. Electrochemically mutable soft metasurfaces. *Nat. Mater.* **24**, 205–211 (2025).
17. Daeyeon, W. et al. Laser-induced wet stability and adhesion of pure conducting polymer hydrogels. *Nat. Electron.* **7**, 475–486 (2024).
18. Keene, S. T. et al. A biohybrid synapse with neurotransmitter-mediated plasticity. *Nat. Mater.* **19**, 969–973 (2020).
19. Lee, Y. et al. A low-power stretchable neuromorphic nerve with proprioceptive feedback. *Nat. Biomed. Eng.* **7**, 511–519 (2023).
20. Wang, W. et al. Neuromorphic sensorimotor loop embodied by monolithically integrated, low-voltage, soft e-skin. *Science* **380**, 735–742 (2023).
21. Hofmeister, F. Zur lehre von der wirkung der salze: zweite mittheilung. *Arch. Exp. Pathol. Pharmakol.* **24**, 247–260 (1888).
22. Nanou, E. & Catterall, W. A. Calcium channels, synaptic plasticity, and neuropsychiatric disease. *Neuron* **98**, 466–481 (2018).
23. Li, H. et al. Electrically weldable conductive elastomers. *Sci. Adv.* **10**, eadp0730 (2024).
24. He, H. et al. Enhancement in the mechanical stretchability of PEDOT:PSS films by compounds of multiple hydroxyl groups for their application as transparent stretchable conductors. *Macromolecules* **54**, 1234–1242 (2021).
25. Gregory, K. P., Wanless, E. J., Webber, G. B., Craig, V. S. J. & Page, A. J. The electrostatic origins of specific ion effects: quantifying the Hofmeister series for anions. *Chem. Sci.* **12**, 15007–15015 (2021).
26. Hua, M. T. et al. Strong tough hydrogels via the synergy of freeze-casting and salting out. *Nature* **590**, 594–599 (2021).
27. Jin, Y. et al. Time-salt type superposition and salt processing of poly(methacrylamide) hydrogel based on Hofmeister series. *Macromolecules* **57**, 2746–2755 (2024).
28. Zhang, Y. et al. Effects of Hofmeister anions on the LCST of PNIPAM as a function of molecular weight. *J. Phys. Chem. C* **111**, 8916–8924 (2007).
29. Wu, S. et al. Poly(vinyl alcohol) hydrogels with broad-range tunable mechanical properties via the Hofmeister effect. *Adv. Mater.* **33**, 2007829 (2021).
30. Ohm, Y., Liao, J., Luo, Y., Ford, M. J. J. & Majidi, C. Reconfigurable electrical networks within a conductive hydrogel composite. *Adv. Mater.* **35**, 2209408 (2023).
31. Geng, Y. et al. A general strategy for exceptionally robust conducting polymer-based bioelectrodes with multimodal capabilities through decoupled charge transport mechanisms. *Adv. Mater.* **37**, e2417827 (2025).
32. Kim, T. Y. et al. Lubricant-infused polymeric interfaces: a stretchable and anti-fouling surface for implantable biomaterials. *Adv. Funct. Mater.* **34**, 2312740 (2023).
33. Hu, R. et al. High-fidelity bioelectrodes with bidirectional ion-electron transduction capability by integrating multiple charge-transfer processes. *Adv. Mater.* **36**, e2403111 (2024).
34. Hua, M. et al. 4D Printable tough and thermoresponsive hydrogels. *ACS Appl. Mater. Interfaces* **13**, 12689–12697 (2021).
35. Zhao, Y. et al. Hierarchically structured stretchable conductive hydrogels for high-performance wearable strain sensors and supercapacitors. *Matter* **3**, 1196–1210 (2020).
36. Zheng, S. et al. Pressure-stamped stretchable electronics using a nanofibre membrane containing semi-embedded liquid metal particles. *Nat. Electron.* **7**, 576–585 (2024).

Acknowledgements

This work was supported by the National Nature Science Foundation of China (Grant No. 52203002 (B.Y.), 52072177 (J.F.), and 52272084 (J.F.)), the Fundamental Research Funds for the Central Universities (Grant No. 30923010204 (B.Y.), 30918012201 (J.F.), 2023102003 (J.F.) and 30919011405 (J.F.)), and the National Key Research and Development Program of China (2022YFB3808800 (J.F.)).

Author contributions

B.Y. and J.F. initiated the concept and designed the overall studies. W.Z., H.Z., Z.L., S.Z., and W.S. led the experiments and collected the overall data. Z.L. and Y.G. contributed to the fabrication of microelectrodes. Z.W. contributed to the small-angle X-ray scattering spectroscopy characterization. All authors contributed the data analysis and provided feedback on the manuscript.

Competing interests

The authors declare no competing interests.

Additional information

Supplementary information The online version contains supplementary material available at https://doi.org/10.1038/s41467-025-68088-3.

Correspondence and requests for materials should be addressed to Bowen Yao or Jiajun Fu.

Peer review information *Nature Communications* thanks Yuanwen Jiang, and the other, anonymous, reviewer(s) for their contribution to the peer review of this work. A peer review file is available.